Non-Bloch-Siegert-type power-induced shift of two-photon electron spin resonances in organic light-emitting diodes

S. I. Atwood,[1] S. Hosseinzadeh,[1] V. V. Mkhitaryan,[2] T. H. Tennahewa,[1] H. Malissa,[1,2] W. Jiang,[3] T. A. Darwish,[4] P. L. Burn,[3] J. M. Lupton,[1,2] and C. Boehme[1]

[1]*Department of Physics and Astronomy, University of Utah, Salt Lake City, Utah 84112, USA*

[2]*Institut für Experimentelle und Angewandte Physik, Universität Regensburg, Universitätsstrasse 31, 93053 Regensburg, Germany*

[3]*Centre for Organic Photonics & Electronics, School of Chemistry and Molecular Biosciences, The University of Queensland, Brisbane, QLD 4072, Australia*

[4]*National Deuteration Facility, Australian Nuclear Science and Technology Organization (ANSTO), Lucas Heights, NSW 2234, Australia and Faculty of Science and Technology, University of Canberra, Canberra, ACT 2617, Australia*

(Received 24 October 2023; revised 19 August 2024; accepted 3 September 2024; published 19 November 2024)

We present Floquet theory based predictions and electrically detected magnetic resonance (EDMR) experiments to elucidate the nature of multiphoton magnetic resonance shifts of charge-carrier spin states in films of the perdeuterated π-conjugated polymer poly[2-(2-ethylhexyloxy-d_{17})-5-methoxy-d_3-1,4-phenylenevinylene-d_4] (d-MEH-PPV) under strong magnetic resonant drive conditions (radiation amplitude B_1 comparable to Zeeman field B_0). Room-temperature, continuous-wave EDMR experiments on d-MEH-PPV-based, electroluminescent, bipolar-injection diodes [i.e., organic light-emitting diodes (OLEDs)] confirm the ability of a nonperturbative numerical method to make quantitative predictions of two-photon resonance shifts in such devices. Additional numerical simulations show that the two-photon resonance shift with increasing power is nearly the same under both linearly and circularly polarized drive, in contrast to the one-photon shift, which only occurs under conditions of noncircularly polarized drive. We therefore treat the Floquet Hamiltonian analytically using arbitrary amplitudes of the co- and counterrotating components of the radiation field to gain insight into the nature of the polarization dependence of multiphoton resonance shifts. The results show that multiphoton resonance shifts depend on both the co- and counterrotating components of an arbitrarily polarized drive field, whereas the one-photon shift depends only on the counterrotating component.

DOI: 10.1103/PhysRevB.110.195304

I. INTRODUCTION

Multiphoton transitions of magnetic dipoles and drive-induced resonance peak shifts are hallmark phenomena of magnetic resonance in the *strong-drive* regime, in which the magnetic resonant drive field amplitude B_1 is comparable in magnitude to the static magnetic Zeeman field B_0 [1–3]. Bloch and Siegert pioneered the description of the drive-induced resonance shift of one-photon resonances, showing that the shift arises when the drive field deviates from circular polarization, i.e., when the field polarization acquires a counterrotating component [3]. Their treatment of one-photon resonances was implicit and without apparent consideration of the possibility of multiphoton resonances, since the earliest experimental multiphoton resonances were only reported a decade after their seminal publication in 1940 [4–6]. Subsequent work has treated multiphoton conditions under a range of limiting approximations [7–9], with studies particularly focusing on scenarios where both two-photon transitions and magnetic resonance peak-center shifts are evident under strong drive. Figure 1 depicts (a) the two-photon transition and (b) a drive field induced resonance shift for purely Zeeman-split electron spin states under conditions of field-swept, continuous-wave (cw) magnetic resonance spectroscopy. Early qualitative indications for shifts in two- and three-photon magnetic dipole transitions emerged from studies on optically pumped sodium by Margerie and Brossel [10]. Shortly after that observation, a theory explaining these transitions was put forward by Winter [11] and further developed by Cohen-Tannoudji and Haroche [12,13]. A qualitatively different observation technique was utilized by Morozov *et al.*, who reported findings for qualitative two- and three-photon shifts in radical-ion pairs of aromatic acceptors in liquids using optically detected magnetic resonance (ODMR) experiments [14]. Recently, Sun *et al.* conducted optical magnetic resonance measurements on ^{133}Cs atoms and quantitatively analyzed two- and three-photon resonance shifts [15]. Similarly, Fregenal *et al.* observed peak shifts in many higher multiphoton transitions while studying n-photon resonances through detection by selective field ionization, with n reaching up to 23 for high orbital angular momentum states in Li Rydberg atoms [16].

In recent years, the exploration of strong drive induced electron spin-resonance shifts using electrically detected magnetic resonance (EDMR) has gained traction. Analogous to ODMR, EDMR enables the observation of electron spin resonances in scenarios of minimal thermal spin polarization. This is achieved by detecting the spin-permutation symmetry of weakly bound electron-hole spin pairs, termed polaron pairs (PPs), which are prevalent, for example, in recombination currents of organic semiconductors [17]. Despite the inherently paired nature of these PPs, their weak spin-spin interaction typically allows the individual charge carriers to behave largely as uncoupled electron spins. This unique

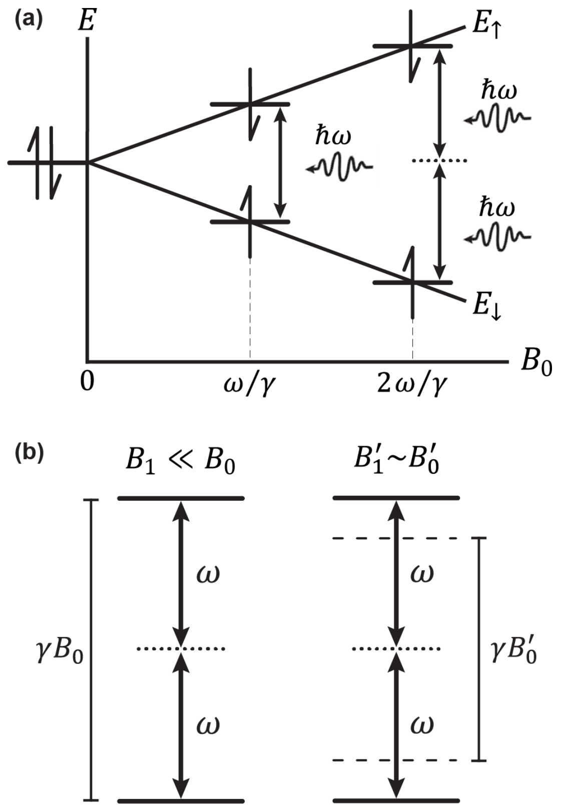

FIG. 1. Conceptual representations of a two-photon transition and drive field induced resonance peak shift. (a) One- and two-photon resonances between quantum spin states of energy E in a static magnetic field B_0 and an oscillating magnetic field with amplitude B_1 and frequency $\omega/2\pi$; γ is the gyromagnetic ratio and $\hbar$ the reduced Planck constant. (b) Energy level diagram in frequency units showing the drive field induced resonance shift of the two-photon resonance, which, under the conditions of field-swept, cw magnetic resonance spectroscopy, requires a reduced Zeeman splitting to maintain the resonance condition with a drive field of constant frequency. Left: For spin states that are weakly coupled to their environment, the eigenenergy level splitting is governed by the Zeeman effect and increases linearly with B_0. Thus a two-photon magnetic resonance can occur at twice the fundamental resonance $B_0 = \omega/\gamma$. Right: Under strong-drive conditions, where $B_1' \sim B_0'$, the energy levels are pushed further apart. The energy of two photons thus matches the renormalized level spacing at a reduced field $B_0' < B_0$, so that the two-photon resonance line shifts toward $B_0 = 0$.

behavior renders EDMR a preferred technique for studying drive-induced magnetic resonance phenomena [1,2,18,19]. Key studies have been performed by Ashton and Lenahan on two-photon resonances in 4H-SiC transistors [2] and by Jamali *et al.*, who identified an apparent resonance at twice the field of the fundamental resonance in an organic semiconductor [18] as a two-photon transition [1]. Both studies highlighted peak shifts under strong drive but stopped short of providing a comprehensive quantitative analysis connecting the observed shifts with existing theoretical descriptions. Jamali *et al.* showed that strong-drive processes can be described via a nonperturbative approach using Floquet analysis of the time-dependent Hamiltonian [1]. Their numerical Monte Carlo simulations exhibited qualitative congruence with experimental EDMR spectra, shedding light on several strong-drive magnetic resonance phenomena. Yet, due to calibration limits for the static magnetic field B_0 and potential interference from overlapping one-photon spin resonances induced by higher harmonics of the rf amplifier, as elaborated upon previously [18], a comprehensive quantitative analysis of the subtle peak-center shifts has been lacking, with a consequent gap in the validation of existing theoretical predictions.

In this work, our focus is to validate the predictive ability of the nonperturbative numerical method in Ref. [1] through improved EDMR measurements and then to apply both the numerical method and a Floquet analysis to explore the nature of multiphoton shifts in electron spin resonance. Our work confirms that the one-photon shift depends only on the counterrotating component of the drive-field polarization, as Bloch and Siegert predicted [3], but reveals that *any* multiphoton resonance shift depends on both the co- and counterrotating components. Our results motivate further studies of multiphoton resonance shifts and other nonlinear behaviors under strong magnetic resonant drive conditions—with regard to both their fundamental nature and their potential applicability for coherent control sequences and quantum-enhanced technological applications such as spin-based quantum sensing.

II. EXPERIMENTAL VALIDATION OF THE NONPERTURBATIVE NUMERICAL METHOD

Jamali *et al.* introduced a numerical simulation tool to predict changes in recombination current from the steady state, at room temperature and under constant bias, induced by weakly dipole- and exchange-coupled spin-1/2 electron-hole charge-carrier PPs in π-conjugated, polymer-based organic bipolar-injection diodes, which also function as light-emitting diodes, i.e., organic LEDs (OLEDs) [1]. The simulation tool exploits a nonperturbative analytical expression for the EDMR signal derived from the Floquet theory based treatment of the stochastic Liouville equation and offers quantitative numerical predictions for single- and multiphoton line shifts and their dependencies on the drive field amplitude B_1. While precise control of B_1 during measurements should substantiate the accuracy of these predictions, there are technical challenges. Even with EDMR, which allows access to electron spin-resonance conditions where $B_0 \sim B_1$ [1,2,18,19], resonance shifts induced by drive power are small in comparison to both the Zeeman splitting of the charge-carrier spin and the resonance linewidths dominated by random hyperfine fields of protonated organic semiconductors [20]. In order to mitigate the latter for a quantitative study of the shifts, we followed the precedent in Ref. [1] and constructed diodes from the perdeuterated π-conjugated polymer poly[2-(2-ethylhexyloxy-d_{17})-5-methoxy-d_3-1,4-phenylenevinylene-d_4] (d-MEH-PPV) [cf. Fig. 2(a)], in which the hydrogen atoms had been isotopically substituted with deuterium [21]. Due to the approximately three times smaller nuclear magnetic moment of deuterium (0.433×10^{-26} J/T vs 1.41×10^{-26} J/T in the case of hydrogen [22,23]), the distribution of Larmor frequencies in d-MEH-PPV is much narrower, so that inhomogeneous broadening of magnetic resonance lines is also smaller and

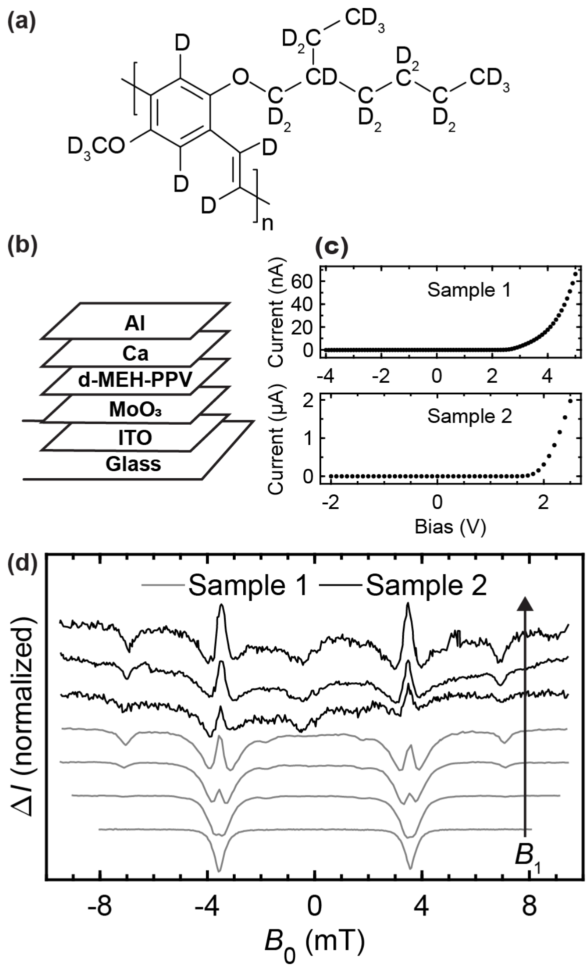

FIG. 2. EDMR spectra of the d-MEH-PPV diodes. (a) Chemical structure of d-MEH-PPV (see Supplemental Material in Ref. [21]). (b) Schematic of a diode. The glass substrate is $(50\times3\times1)$ mm^3 and has lithographically defined electrodes. (c) Current-voltage measurements of two different d-MEH-PPV-based diodes, samples 1 and 2, based on the structure shown in (b), yet with different active areas (5 mm^2 and 0.8 mm^2, respectively). (d) A selection of EDMR spectra from samples 1 and 2 measured at high rf power (frequency 100 MHz), with B_1 increasing from bottom to top (cf. Ref. [30] for the full dataset). Each spectrum is baseline corrected, normalized, and offset on the y axis for clarity. The field B_0 was calibrated using the one-photon resonance at low drive fields (not shown) as reference. The measurements took place at different yet overlapping power intervals. Two-photon resonances, as well as signatures of spin collectivity (the spin-Dicke effect [19]), indicated by the bifurcation of the one-photon resonance, become apparent at higher powers, i.e., at and above the third spectrum from the bottom.

therefore the EDMR signals are larger compared to the protonated materials. This effect improves the signal to noise ratio (SNR) of weak nonlinear resonance lines and reduces the overlap of neighboring lines that can complicate line center analysis. The use of d-MEH-PPV therefore allowed us to observe two-photon resonances at weaker B_1 fields and estimate the resonance line centers—and thus their shifts—more accurately.

Our detection scheme followed those of previous room-temperature cw experiments (see Experimental Setup in the Appendix) [1,18,19], but with the following two changes to allow quantitative analysis of the line center shifts: (i) we inserted a low-pass filter to remove amplifier harmonics and consequent one-photon harmonic resonances that might superimpose on multiphoton resonances, and (ii) we conducted bidirectional field sweeps to allow accurate calibration of the field B_0 (see Experimental Data Analysis in the Appendix). We also implemented sinusoidal rf-amplitude modulation with lock-in detection to separate the magnetic resonance induced, spin-dependent electrical current from radiation-induced, spin-independent electrical currents. Figure 2(b) shows the layer structure of the d-MEH-PPV-based diodes, which were fabricated as previously reported [19,24–26]. Data were collected from two different d-MEH-PPV samples, labeled 1 and 2. Sample 1 had a larger active area (5 mm^2) compared to sample 2 (0.8 mm^2) and thus a better SNR, while the smaller area of sample 2 improved heat dissipation and homogeneity of the applied magnetic fields across the active area of the device, both of which were advantageous in experiments at high rf-drive fields.

When the diodes are under voltage bias, PPs form in the polymer layer from free charge carriers and then either dissociate back into free charge carriers or recombine into tightly bound excitons [27,28]. Our EDMR-detection approach allows us to measure changes in the electrical current resulting from changes in the steady-state populations of singlet and triplet PPs under resonant spin excitation [19,29]. In Fig. 2(c), the exponential behavior of current-voltage measurements on the samples verifies their rectifying behavior as diodes and strongly suggests recombination of PPs. Light emission (electroluminescence) occurs secondarily through the annihilation of singlet excitons in a step that follows after the polaron pairs recombine [24]. Since electrical current is the experimental observable in this study, electroluminescence data were not recorded (see further discussion in Sec. IV).

Figure 2(d) shows a selection of the spectra recorded at high rf power (frequency 100 MHz) with samples 1 and 2, with baseline correction applied as well as calibration of B_0 (see Experimental Data Analysis in the Appendix). All spectra collected from the samples are shown in the Supplemental Material [30]. The spectra from each sample cover different but overlapping ranges of B_1 and are stacked from bottom to top in order of increasing B_1, which was estimated by assuming a linear relationship between B_1 and the rf amplitude (see Estimating B_1 in the Appendix). The data from sample 1 exhibit superior SNR, as described above. In the third spectrum from the bottom, a two-photon resonance is clearly visible at approximately $|B_0| = 7$ mT, and the one-photon resonance peak at approximately $|B_0| = 3.5$ mT has inverted, a signature of the spin-Dicke effect [19]. The linewidths are primarily convolutions of Gaussian hyperfine-field distributions and Lorentzian power broadening, the latter making the dominant contribution under strong drive. Under weak-drive conditions, not shown in Figure 2(d), the line shapes consist of superpositions of two Gaussian distributions with full-width-half-maxima (FWHM) of (0.178 ± 0.001) mT and (0.574 ± 0.004) mT [21] corresponding to inhomogeneous broadening from each spin species in the PP [18,19,31]. Although these factors are relevant to the line shapes, our simulations lead us to conclude that they have no sizable effect

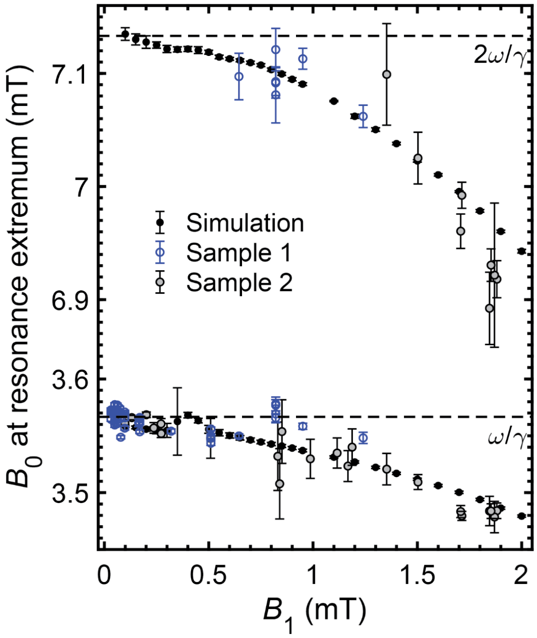

FIG. 3. Plots of the one- and two-photon d-MEH-PPV resonance peak extrema as a function of B_1, on scales of B_1 determined by the best-fit match of the experimental and numerical one-photon peak extrema (see Estimating B_1 in the Appendix). The horizontal dashed lines mark the hypothetical unshifted peak centers.

on the resonance *shifts*, which are the focus of the current study.

Figure 3 shows the estimated values of B_0 where local extrema occurred, corresponding to the one- and two-photon resonance centers of the experimental data, plotted as a function of B_1, from all recorded spectra [30]. We estimated the line centers with the local extrema of the EDMR resonances due to the absence of analytical expressions for the individual EDMR resonances that emerge in the strong-drive regime, with the understanding that the local extrema do not always coincide with resonance line centers, e.g., when line shapes are asymmetric or resonance lines overlap. While the experimental results from samples 1 and 2 cover different ranges of B_1, all the data consistently exhibit resonance line center shifts with increasing B_1. In addition, Fig. 3 displays local extrema from numerical simulations of the EDMR spectra of d-MEH-PPV using the nonperturbative method in Ref. [1] (the simulated spectra can be viewed in the Supplemental Material [30]). For computational efficiency, we performed the numerical simulations under the assumption of square-wave modulation rather than sinusoidal modulation, having verified that the line centers under both methods were consistent within the error range (see Numerical Data Analysis in the Appendix). The numerical one-photon peak centers show an irregular feature at $B_1 = 0.4$ mT, where the one-photon resonance peak becomes ill defined due to the onset of the spin-Dicke effect [19]. Overall, the numerical data show agreement not only with the one-photon experimental values, but also with the two-photon values. This agreement confirms the underlying Floquet model and validates the use of the nonperturbative numerical method to study nonlinear EDMR spectra, particularly the nature of the two-photon shift and higher multiphoton shifts.

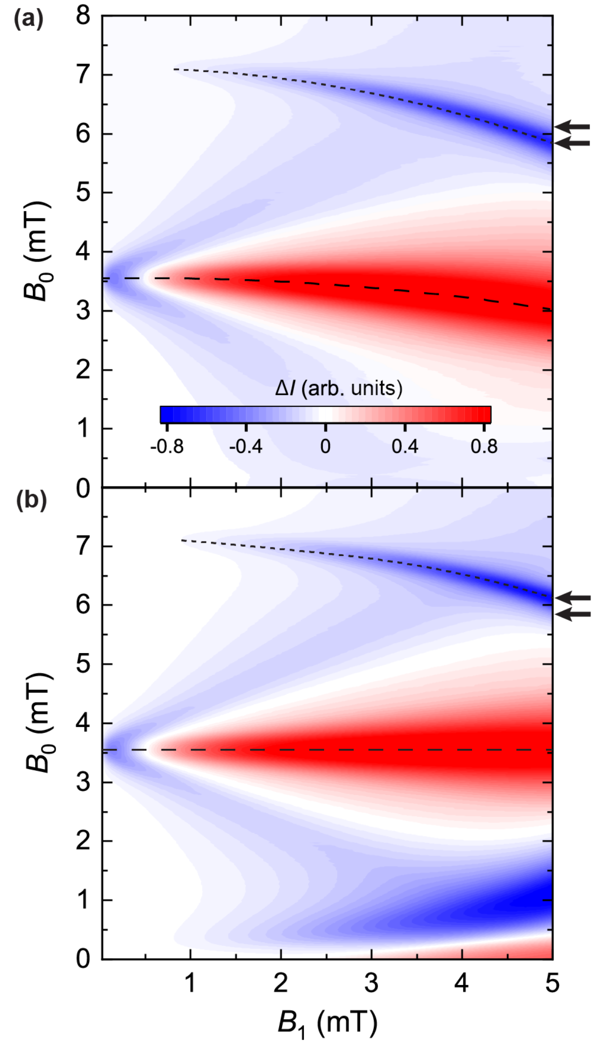

FIG. 4. Simulated change ΔI to the steady-state d-MEH-PPV diode current as a function of B_0 and B_1 under (a) linearly and (b) circularly polarized rf field with frequency of 100 MHz. The dashed lines are a guide to the eye for the one-photon and two-photon resonance peak centers. The pairs of arrows are placed at identical magnetic field values in (a,b) and mark the difference of the two-photon peak center at $B_1 = 5$ mT under linear and circular polarization. Under linear polarization, drive amplitude induced shifts are visible for both one- and two-photon resonances, while under circular polarization, there is no shift of the one-photon resonance, as expected from the analysis of Bloch and Siegert. Importantly, the shift of the two-photon resonance remains under circular polarization, albeit slightly weaker.

III. THEORETICAL STUDY OF MULTIPHOTON RESONANCE SHIFTS

Our theoretical study of multiphoton resonance shifts involves extensive numerical simulations of EDMR spectra using the nonperturbative method validated in the previous section. Figure 4 displays a comparison between simulations of the diode current as a function of B_0 and B_1 for (a) linearly and (b) circularly polarized strong rf excitation. The numerical data show that the one-photon resonance shift observed under linear excitation disappears under circularly polarized (CP) excitation. This behavior is consistent with the prediction of Bloch and Siegert that the one-photon shift requires the presence of a counterrotating, off-resonant component of B_1 [3], which is present in a linearly polarized (LP) field but not in a purely CP field. In contrast, the two-photon shift remains nearly unchanged for both LP and CP excitation, with a small difference indicated by the two black arrows in Fig. 4. This behavior suggests that the underlying dependence on field polarization of the two-photon resonance shift is different from that of the one-photon shift. Simple polarization-based arguments show that in two-level systems under magnetic resonance with the static field $\mathbf{B}_0$ perpendicular to the drive field $\mathbf{B}_1$, only odd-photon transitions may occur, while even-photon transitions become possible when the angle between $\mathbf{B}_0$ and $\mathbf{B}_1$ is tilted away from 90° [32]. A thorough analysis of the tilt-angle dependence of one- and two-photon transitions was given in Ref. [9], based on the Floquet-theory approach [7]. We therefore extend the analysis of Ref. [9] to gain insight into the origin of the multiphoton resonance shifts and to interpret the numerical results.

We consider a single spin $S = 1/2$ in a hyperfine magnetic field $\mathbf{B}_{\rm hf}$, which results from unresolved hyperfine couplings between the electronic spins of the PPs and the surrounding nuclear spins, and externally applied static and rf magnetic fields, $\mathbf{B}_0 = B_0\hat{\mathbf{z}}$ and $\mathbf{B}_{\rm rf} = B_{\rm rf}\cos(\omega t)\hat{\mathbf{x}}$, respectively. To simplify the calculations, we align the quantization axis $\hat{\mathbf{z}}$ with the total static field, $\mathbf{B}_0 + \mathbf{B}_{\rm hf}$, and place $\mathbf{B}_{\rm rf}$ in the xz plane. The angle θ between the new x axis and the driving field $\mathbf{B}_{\rm rf}$ is expressed through the original x component of the hyperfine field as $\sin\theta = B_{{\rm hf},x}/|\mathbf{B}_0 + \mathbf{B}_{\rm hf}|$. The energies of the two Zeeman-split levels are $E_\alpha = -\gamma|\mathbf{B}_0 + \mathbf{B}_{\rm hf}|/2$ and $E_\beta = +\gamma|\mathbf{B}_0 + \mathbf{B}_{\rm hf}|/2$, where γ is the gyromagnetic ratio. The Floquet Hamiltonian [7] in the basis of dressed Floquet states, $\cdots, |\alpha,-1\rangle, |\beta,-1\rangle, |\alpha,0\rangle, |\beta,0\rangle, |\alpha,1\rangle, |\beta,1\rangle, \cdots$, is

$$\begin{pmatrix} \cdot & \cdot & \cdot & \cdot & \cdot & \cdot & \cdot & \cdot \\ \cdot & E_\alpha-\omega & 0 & r_{11} & r_{12} & 0 & 0 & \cdot \\ \cdot & 0 & E_\beta-\omega & r_{21} & r_{22} & 0 & 0 & \cdot \\ \cdot & r_{11}^* & r_{21}^* & E_\alpha & 0 & r_{11} & r_{12} & \cdot \\ \cdot & r_{12}^* & r_{22}^* & 0 & E_\beta & r_{21} & r_{22} & \cdot \\ \cdot & 0 & 0 & r_{11}^* & r_{21}^* & E_\alpha+\omega & 0 & \cdot \\ \cdot & 0 & 0 & r_{12}^* & r_{22}^* & 0 & E_\beta+\omega & \cdot \\ \cdot & \cdot & \cdot & \cdot & \cdot & \cdot & \cdot & \cdot \end{pmatrix}. \tag{1}$$

Introducing CP corotating and counterrotating components of rf, B_1 and $\bar{B}_1$, the off-diagonal elements of Eq. (1) are

$$\begin{aligned} r_{11} &= \frac{1}{8}\gamma\left(B_1 + \bar{B}_1\right)\sin\theta, \\ r_{12} &= \frac{1}{4}\gamma\left[\bar{B}_1\cos^2\frac{\theta}{2} - B_1\sin^2\frac{\theta}{2}\right], \\ r_{21} &= \frac{1}{4}\gamma\left[B_1\cos^2\frac{\theta}{2} - \bar{B}_1\sin^2\frac{\theta}{2}\right], \\ r_{22} &= -r_{11}. \end{aligned} \tag{2}$$

Typically, the tilt angle θ is small, so that r_{12} predominantly corresponds to the counterrotating component of rf, and r_{21} to the corotating component. The diagonal elements r_{11} and r_{22} correspond to a component of rf that is parallel to the quantization axis due to the nonzero tilt.

We treated Eq. (1) with the perturbative approach introduced in Ref. [7] to obtain expressions for the shifts and intensities of one- and multiphoton resonances (see Floquet Analysis in the Appendix). The one-photon shift is given by

$$\begin{aligned} \gamma B_{\gamma_1} &= \omega + 2\frac{|r_{12}|^2}{E_\alpha - E_\beta - \omega} \\ &\simeq \omega - \frac{|r_{12}|^2}{\omega}; \end{aligned} \tag{3}$$

i.e., at $\theta = 0$, it depends only on the counterrotating field component B_1, consistent with the result from Bloch and Siegert [3]. For the n-photon transition ($n \geqslant 2$), the resonance condition is

$$\begin{aligned} \gamma B_{\gamma_n} &= n\omega + 2\left[\frac{|r_{12}|^2}{E_\alpha - E_\beta - \omega} + \frac{|r_{21}|^2}{E_\alpha - E_\beta + \omega}\right] \\ &\simeq n\omega - 2\left[\frac{|r_{12}|^2}{(n+1)\omega} + \frac{|r_{21}|^2}{(n-1)\omega}\right]. \end{aligned} \tag{4}$$

These expressions reveal the source of the dependence on field polarization of the two-photon shift in Fig. 4: *any* multiphoton shift depends on both the co- and counterrotating components of the drive field. Moreover, for an LP field, i.e., $\bar{B}_1 = B_1$, the corotating term makes a greater contribution because of the $n-1$ factor in the denominator and is most heavily weighted at $n = 2$. As n approaches infinity, the contributions from both the co- and counterrotating components approach zero. Additional insight can be gained by examining the Floquet Hamiltonian in Eq. (1): multiphoton resonance shifts depend on the corotating component of the field because multiphoton transitions occur through intermediate Floquet states, whereas the one-photon transition occurs directly between Floquet states.

The experimental and numerical data in Fig. 3 can be compared against Eqs. (3) and (4) under conditions of linear field polarization. Using Eq. (2) with $\bar{B}_1 = B_1$ (LP rf field), we get

$$\begin{aligned} B_{\gamma_1} &\simeq \frac{\omega}{\gamma} - \frac{\gamma B_1^2\cos^2\theta}{16\omega}, \\ B_{\gamma_n} &\simeq n\frac{\omega}{\gamma} - \frac{\gamma B_1^2\cos^2\theta}{4\omega}\frac{n}{n^2-1}, \quad \text{for } n \geqslant 2, \end{aligned} \tag{5}$$

implying that for any LP amplitude of B_1, the ratio of the shift of an n-photon resonance ($n \geqslant 2$) and the one-photon resonance must be

$$\frac{\Delta B_{\gamma_n}}{\Delta B_{\gamma_1}} = \frac{n\frac{\omega}{\gamma} - B_{\gamma_n}}{\frac{\omega}{\gamma} - B_{\gamma_1}} = \frac{\frac{\gamma B_1^2\cos^2\theta}{4\omega}\frac{n}{n^2-1}}{\frac{\gamma B_1^2\cos^2\theta}{16\omega}} = \frac{4n}{n^2-1}, \tag{6}$$

where $\Delta B_{\gamma_m} \equiv m\omega/\gamma - B_{\gamma_m}$ for $m \geqslant 1$. This result depends only on the number of photons in the n-photon resonance being tested. For the two-photon shift, the predicted ratio is $8/3 \approx 2.67$.

Figure 5 shows, as a function of B_1, the ratios of shifts from Eq. (6), $\Delta B_{\gamma_2}/\Delta B_{\gamma_1} = (2\omega/\gamma - B_{\gamma_2})/(\omega/\gamma - B_{\gamma_1})$, from the

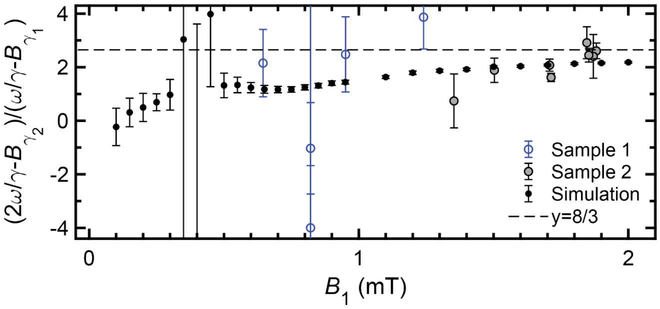

FIG. 5. Ratios of one- and two-photon resonance shifts vs B_1. The ratios $\Delta B_{\gamma_2}/\Delta B_{\gamma_1} = (2\omega/\gamma - B_{\gamma_2})/(\omega/\gamma - B_{\gamma_1})$ were calculated from Eq. (6) with the numerical and experimental spectra represented in Fig. 3 that have both one- and two-photon resonances [30]. The horizontal dashed line is the analytically predicted value of 8/3. The vertical range is restricted to examine the data close to the horizontal line; a figure with the full range is provided in the Supplemental Material [30].

numerical and experimental spectra represented in Fig. 3 that have both one- and two-photon resonances [30]. This allows us to evaluate (i) whether the ratios agree with the predicted value of 8/3 and (ii) whether they are independent of B_1. The ratios from simulations are not 8/3 for small values of B_1, yet they approach 8/3 with increasing B_1. The deviation at small values of B_1 can be attributed to the absence of hyperfine disorder in Eq. (6) and to our use of the peak extrema to approximate the line centers, especially near where the spin-Dicke effect inverts the one-photon resonance, i.e., where the extremum is poorly defined. Figure 5 suggests that the approximation becomes better as B_1 increases and the inversion approaches saturation [33]. The ratios from the experimental data follow the simulations at higher values of B_1, whereas at lower values of B_1, they are consistent with both the simulations and the analytical value of 8/3 but do not unambiguously confirm either because of large uncertainties, which can be traced to shift values that are comparable to or smaller than their respective uncertainties and therefore lead to large uncertainties in the ratios through error propagation.

IV. DISCUSSION AND SUMMARY

Although the experimental observable in this report is the electrical current of an OLED, we see no reason not to expect that the light emission of the OLED will reflect the same strong-drive effects as seen in the electrical currents. The correlation between spin-dependent photon emission rates, i.e., the spin-dependent changes to the light intensity of the devices studied here, have been shown to correlate closely with the spin-dependent electrical currents driving the electroluminescence [24]. This correlation has been corroborated for many active materials in OLEDs, not just through magnetically resonant spin manipulation by comparison of ODMR and EDMR experiments [24,34], but also through magnetoresistance and magnetoelectroluminescence experiments [35,36]. These previous experiments confirm that spin-dependent recombination affects both the electrical current and electroluminescence. Given that the goal of our study was not to corroborate the correlation of electrical current and optical emission, we focused on EDMR measurements, which are experimentally less challenging.

In summary, we report the experimental observation of power-induced shifts in one- and two-photon magnetic-dipole resonances in EDMR at low magnetic field and low frequency. The experiments utilize spin-dependent electrical recombination currents through electron-hole PP states in diodes with perdeuterated MEH-PPV as the active layer and also make use of lock-in detection, bidirectional field sweeps, and a low-pass filter, which removes undesired harmonics generated by the rf amplifier. These adjustments allow for quantitative estimations of the resonance peak shifts, which validate a nonperturbative, Floquet theory based numerical method for simulating nonlinear EDMR spectra in the diodes [1]. Simulations generated by the same numerical method show that, unlike for the case of the one-photon shift, the two-photon shift only weakly depends on the field polarization. A separate perturbative analysis of the Floquet Hamiltonian [7] confirms the prediction by Bloch and Siegert [3] that the one-photon shift depends only on the counterrotating component of the field polarization and also shows that multiphoton resonance shifts depend on both the co- and counterrotating components. While the analysis predicts that the ratios of shifts are independent of B_1, the shifts obtained from simulations deviate from the analytical prediction of 8/3 [cf. Eq. (6)] at low B_1. We can attribute this deviation to the absence of hyperfine disorder in Eq. (6) and to our method of determining the peaks via the local extrema. The experimental ratios obtained in this study are consistent with the simulations at higher values of B_1 but are insufficient to confirm the deviation between the simulations and the analytical prediction at lower values. Our results call for additional experiments to test the predicted dependence of multiphoton resonance shifts and intensities on field polarization and on the relative orientation of B_1 and B_0, as well as the relationship between the nonperturbative numerical simulations and the perturbative analytical predictions. Experimental results validating the analytical predictions of Eq. (6) for three-photon spin resonances have recently been published [37].

ACKNOWLEDGMENTS

This work was supported by the U.S. Department of Energy, Office of Basic Energy Sciences, Division of Materials Sciences and Engineering under Award No. DE-SC0000909. H.M. and V.V.M. acknowledge support from the Deutsche Forschungsgemeinschaft (DFG, German Research Foundation) (Project ID No. 314695032—SFB 1277, subproject No. B03). The synthesis of the perdeuterated monomer took place at the Australian National Deuteration Facility, which is partly funded by NCRIS, an Australian Government initiative. P.L.B. was an Australian Research Council Laureate Fellow, and the synthesis work was supported in part by this Fellowship (FL160100067).

APPENDIX

1. Experimental setup

The experiment consisted of sweeping the field B_0 bidirectionally under a cw field B_1 (frequency 100 MHz) and recording (i) room-temperature changes to a ∼10 μA steady-

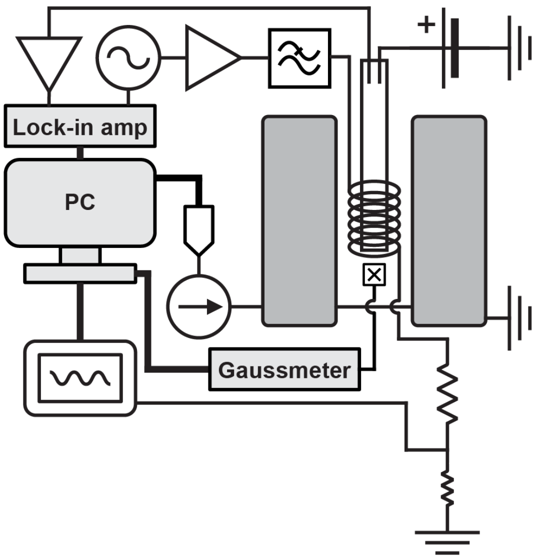

FIG. 6. Illustration of the experimental setup. The two thick, vertical gray bars represent the poles of the electromagnet that generates B_0.

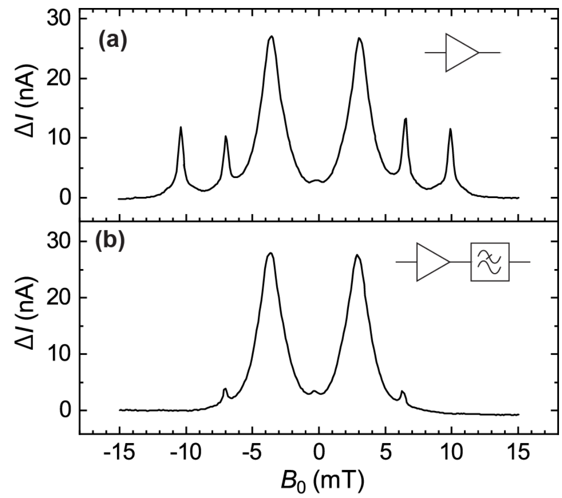

FIG. 7. EDMR spectra of a SY-PPV diode (a) without and (b) with an rf low-pass filter. In (a), resonances appear at $|B_0| \sim 7$ mT and $\sim$10.5 mT, where the two- and three-photon resonances are expected. However, in (b), the resonances at $|B_0| \sim 7$ mT are greatly reduced, while those at $|B_0| \sim 10.5$ mT are completely eliminated. The conclusion is that the supposed two-photon resonances in (a) are superpositions of the two-photon resonance and one-photon harmonics, while the supposed three-photon resonances are in fact entirely one-photon harmonics.

state forward current of a d-MEH-PPV-based diode, (ii) the field B_0, and (iii) the voltage across a sensing resistor connected in series with the rf coil as a measure of B_1. Figure 6 depicts the experimental setup. The circuit used to detect the diode current consists of two 6 V batteries, a Stanford Research Systems SR570 low-noise current amplifier, and a Zurich HF2LI digital lock-in amplifier. The circuit that generates B_0 consists of a Varian V3603 electromagnet, a Kepco 20-20D bipolar power supply, and a National Instruments PI 6221 multifunction I/O device. The magnetic flux between the poles of the electromagnet was measured using a Hall sensor connected to an F. W. Bell Model 5080 gauss meter. The rf circuit consists of a Hewlett Packard 8656B signal generator (modulated by the lock-in amplifier), an ENI 5100L rf amplifier, a Microwave Filter Company 17842-6 low-pass filter (passband 0–120 MHz, nominal 0.5 dB insertion loss, and minimum 50 dB rejection between 127 and 488.5 MHz), a custom-made copper coil surrounding the diode, a Fairview ST3NF50PL 50 Ω termination resistor, and a series sensing resistor consisting of two parallel 1 Ω resistors. The waveform across the sensing resistor was recorded with an Agilent MSO6104A oscilloscope.

As the high power required to produce large cw B_1 pushes rf amplifiers into the nonlinear response domain, higher rf harmonics can arise, requiring rf filtering. To test the ability of the low-pass filter inserted into our cw EDMR setup to suppress resonances caused by higher amplifier harmonics, we recorded EDMR spectra with diodes fabricated from commercially available super-yellow PPV (SY-PPV), which was also used in Ref. [18]. The measured data, shown in Fig. 7, were obtained under strong-drive amplitudes ($B_1 \sim 0.5$ mT) (a) without and (b) with the inclusion of the rf low-pass filter ($f_c \sim 120$ MHz). In (b), the features at the second harmonic at $|B_0| \sim 7$ mT are substantially reduced compared to panel (a), thereby demonstrating the possibility to detect the two-photon resonance without the superimposed contribution of higher rf harmonics. In contrast, the features seen at $|B_0| \sim 10$ mT in panel (a) are eliminated in panel (b), thereby confirming that these features are entirely due to amplifier harmonics rather than three-photon resonances. While theory does predict the existence of three-photon resonances [1], the B_1 amplitude reached in these measurements was too low to observe them. We confirmed through an analysis of the power broadening of the spectra [18] that the attenuation of higher-order resonances was not due to an attenuation of B_1.

We implemented a sinusoidal rf-amplitude modulation scheme of B_1 with phase-sensitive (i.e., lock-in) detection of the sample current, allowing for the separation of the magnetic resonance induced, spin-dependent electrical current from radiation-induced, spin-independent electrical currents. The latter currents contribute random artifact signals, yet they are not strictly noise because they follow the rf-amplitude modulation and therefore cannot be filtered out solely by the narrow bandpass filter behavior of a lock-in amplifier. Nevertheless, it is possible to separate these electrical signals from spin-dependent electrical current signals using a lock-in detector because of their entirely different dynamical signatures. The dynamics of spin-dependent recombination occur at kilohertz to megahertz rates, while the radiation-induced electronic effects are much faster, in the megahertz to gigahertz range. Thus the two signal types can be separated between the in-phase (X) and out of phase (Y) channels by a suitable choice of modulation frequency ($f_s = 1$ kHz) and reference phase. We recorded all spectra using a fixed reference phase and then digitally adjusted the reference phase to minimize the spin-independent contributions in the out of phase channel, which then typically contained only EDMR signal contributions, as depicted in Fig. 8. Due to the arbitrary phase, the absolute signs of the current change [ordinates in Fig. 2(d)] are also arbitrary and have been set to be consistent with

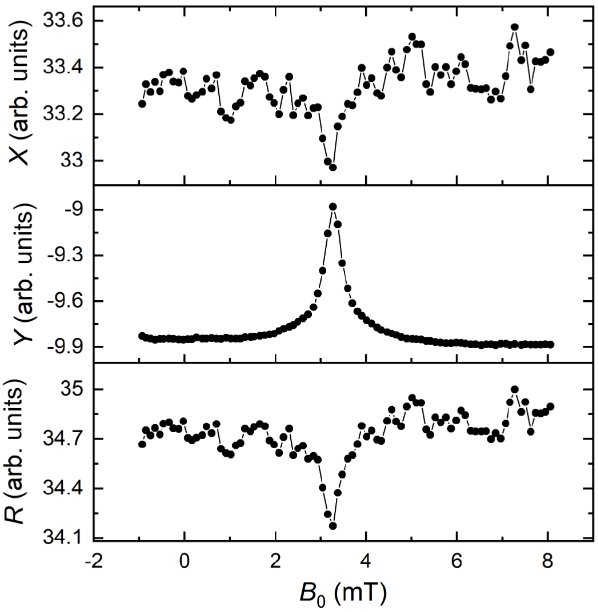

FIG. 8. Low drive power EDMR spectra obtained for the in-phase lock-in channel (top), out of phase channel (center), and absolute (bottom) of both channels. Since spurious electrical signals—not related to magnetic resonance—display significantly faster dynamics, they can be separated by using a modulation frequency higher than the dominant harmonic components of the spin-dependent electrical current measured here for EDMR spectroscopy, yet lower than the harmonic components of the spurious radiation artifact signals. By appropriate choice of the reference phase, the contributions of these spurious signals can be minimized in the out of phase channel (Y), which then typically contains only EDMR signal contributions.

the absolute signs of the simulated spectra [30], which are in turn consistent with experimental EDMR spectra recorded previously through direct detection [1].

2. Experimental data analysis

After the reference phase of the lock-in amplifier had been adjusted, the experimental spectra were analyzed according to the following procedure: first, the signal was subjected to a linear baseline correction to compensate for nonresonant, rf-induced, quasi-static magnetoresistance effects [38]. Second, the EDMR peak centers were determined by second-order polynomial fits to the local extrema. The error reported for each extremum propagated through the covariance matrix of the fit and originated from the noise distribution of the ordinates of the spectra. Third, the peak centers of the one-photon resonance at low resonant drive fields were used to calibrate B_0, following the previously reported robust absolute magnetometry approach based on spin-dependent recombination [39]. During the experiment, we swept the magnetic field B_0 bidirectionally (i.e., recording the EDMR trace for two opposite magnetic-field directions) in order to obtain symmetric one-photon peak centers. We then extracted a linear function consisting of a scaling factor a and an offset constant b, with a being calculated from the one-photon resonance peaks in the low rf power regime, where the peak centers align with the theoretical Zeeman energy of a free electron, ω/γ, and the offset b being determined from the midpoint between the one-photon EDMR peaks. This approach allowed us to obtain a highly accurate calibration of the magnetic field, i.e., the relationship between the value of B_0 measured by the Hall sensor and the actual value of B_0.

3. Estimating B_1

B_1 was estimated by assuming a linear relationship $B_1 = cV$ between B_1 and the rf amplitude V, which is proportional to the square root of the applied power. Given that sample alignment, the resonator quality factor, and the coupling between sample and radiation field are sensitive to small positional changes of the sample relative to the excitation coils and sample holder, the conversion factor c can change dramatically between experiments, for example, when the sample holder is removed from the magnet and a new sample placed into it. The determination of B_1 is therefore most reliably done during the recording of a cw EDMR spectrum. This, however, conflicts with the need to conduct transient spin nutation measurements (the standard way of measuring B_1), which are pulsed electrically detected spin-Rabi oscillation experiments [17,28] and therefore cannot be conducted simultaneously with cw EDMR experiments. To address this problem, we estimated B_1 in two steps. In the first step, we determined a separate c for samples 1 and 2 through a global fit to several spectra in the intermediate-drive regime as described in Ref. [18] and then averaged the two values after verifying that they agreed within two standard deviations. For sample 1, the standard deviation was calculated from the statistics of several fits, while for sample 2, it was calculated through a numerical bootstrapping method [20,40]. We accounted for the effect of sinusoidal modulation [Eq. (A2)] on linewidth by assuming that the system reached a steady state on a timescale much shorter than the modulation period $1/f_s$. Under that assumption, the linewidth modulation averages to zero over the modulation period, so that the time-averaged modulated linewidth can be treated as the unmodulated linewidth. In the second step, we used the one-photon shift to apply a second correction factor to the averaged value c. Given that the shift of the one-photon electron spin resonance has a well-understood dependence on B_1 [3], the numerical Floquet theory predictions for the dependence of the two-photon shift on B_1 can be evaluated against experimental data by comparing their agreement after the experimental one-photon shifts are scaled along the axis of B_1 to match the one-photon numerical predictions (cf. Fig. 3). The second correction factor to c was therefore obtained through a numerical least-squares fit of the experimental one-photon peaks to the numerically simulated one-photon peaks, and this correction factor was then applied to obtain the abscissae of the experimental data shown in Fig. 3.

The procedure described above removed the need to obtain values of B_1 during the measurements. Nevertheless, the value of c for each sample is expected to have changed at high power as ohmic heating effects shifted the overall impedance and tuning of the rf circuit. This uncertainty limits the accuracy of the estimated values of B_1.

4. Numerical data analysis

As with the experimental data, we analyzed the simulated data on the basis of local extrema of the EDMR spectra, fitting the extrema with second-order polynomials. Vertical uncertainty intervals originate from inaccuracies in the magnetic field where local extrema occur, analogous to error bars of experimental data, and were obtained by making an initial fit to the simulated spectra, taking the standard deviation of the residuals, and then fitting the peaks again using the standard deviation to generate a covariance matrix from which the error in the resonance line center was computed.

In preparation for the experimental work, we also studied numerically whether the extrema-based analysis of resonance line-shift data could be affected by the modulation envelope used for lock-in detection. The theoretical treatment of lock-in measurements with sinusoidal modulation of the rf amplitude, which was the experimental configuration, is computationally expensive compared to the treatment of rectangular modulation. In the case of rectangular modulation, the EDMR signal under slow modulation ($f_s = 1$ kHz in our experiments) is proportional to the difference of steady-state diode current with and without the rf drive of amplitude B_1, i.e.,

$$\mathrm{EDMR}(B_0) \propto I(B_1,\ B_0) - I(0,\ B_0). \tag{A1}$$

In this case, the EDMR spectra may be calculated using the truncation scheme described in Ref. [7] by restricting the Floquet degree of freedom to a finite domain, $-N_0 \leqslant n \leqslant N_0$. Thus the truncated Floquet Hilbert space is $4(2N_0 + 1)$-dimensional. The optimal value of N_0 is found by inspecting the convergence of the simulation result against increasing N_0. We have verified numerically that $N_0 = 4$, corresponding to a 36×36 truncated Floquet Hamiltonian, which ensures an acceptable convergence for $I(B_1,\ B_0)$ in the parameter domain of interest. This approach provides a convenient numerical procedure for the calculation of $I(B_1,\ B_0)$ on a standard desktop processor within a reasonable time frame.

In contrast to rectangular modulation, sinusoidal modulation does not allow for a simple interpretation of the EDMR spectra as in Eq. (A1). The rf amplifier output voltage is described by

$$V = V_0 \cos(2\pi f_f t)[1 + m \cos(2\pi f_s t)], \tag{A2}$$

where the carrier frequency $f_f = 100$ MHz and the modulation depth $m = 0.9$. To simulate the corresponding spectra, we decompose the signal described by Eq. (A2) into

$$B_1(t) = B_1\Big[\cos(2\pi f_f t) + \frac{m}{2}\cos[2\pi(f_f + f_s)t] + \frac{m}{2}\cos[2\pi(f_f - f_s)t]\Big], \tag{A3}$$

and consider a system subject to a multifrequency drive involving three asynchronous incident rf fields of frequencies f_f, $(f_f + f_s)$, and $(f_f - f_s)$. The extension of the Floquet theory for this multifrequency drive, Eq. (A3), is straightforward. An additional Floquet degree of freedom is introduced, and the dressed states are expressed as $|\alpha, n_1, n_2\rangle$, with two integers n_1 and n_2 that represent the f_f- and f_s-photon numbers. The truncation is realized by restricting the range of the two integers, $-N_f \leqslant n_1 \leqslant N_f$ and $-N_s \leqslant n_2 \leqslant N_s$, and results in a $4(2N_f + 1)(2N_s + 1)$-dimensional Hilbert space. As above, the optimal values of N_f and N_s are found by testing the convergence of the simulated EDMR spectra. Our simulations show that the necessary convergence is achieved if $N_f, N_s \geqslant 4$. Hence the truncated Hilbert space is at least $4 \times 9^2 = 324$-dimensional. Because of this large size, the numerical simulation of EDMR lines for sinusoidal rf modulation requires extraordinary computational cost compared to simulations for rectangular modulation ($\geqslant 36$-dimensional). We therefore conducted most simulations with rectangular modulation after running a few simulations with sinusoidal modulation for control. Although our simulations reveal that these two modulation modalities impact EDMR line shapes differently, we found that the difference between peak centers (mean difference 6 μT, standard deviation 20 μT for $n = 3$ comparisons) is less than the uncertainty limits of the experimental data (mean uncertainty interval 17 μT, standard deviation 15 μT for $n = 30$ data points).

5. Floquet analysis

Having established the Floquet Hamiltonian in Eq. (1), we consider the situation where the applied frequency ω is nearly resonant with the energy separation of the two states, $E_\beta \approx E_\alpha + \omega$, i.e., the one-photon resonance. Following Shirley [7], we separate the portion of the Floquet Hamiltonian acting on the two nearly degenerate levels as a 2×2 matrix, $\mathcal{H}_2$, and account for the rest of the Hamiltonian approximately by including perturbation corrections to the two nearly degenerate levels and coupling elements thereof from the remaining states. Specifically, we separate the nearly degenerate levels $|\beta, 0\rangle$ and $|\alpha, 1\rangle$ that are nonresonantly coupled with the states $|\alpha, -1\rangle$ and $|\beta, 2\rangle$, respectively. This coupling is given by r_{12}, dominated by the counterrotating component of the rf field. Incorporating this coupling into $\mathcal{H}_2$ using perturbation theory gives

$$\mathcal{H}_2 = \begin{pmatrix} E_\beta + \delta_\beta & r_{21} \\ r_{21}^* & E_\alpha + \delta_\alpha + \omega \end{pmatrix}, \tag{A4}$$

where

$$\delta_\alpha = \frac{|r_{12}|^2}{E_\alpha - E_\beta - \omega} \simeq -\frac{|r_{12}|^2}{2\omega}, \quad \delta_\beta = -\delta_\alpha. \tag{A5}$$

Note that the nonresonant interactions among the states $|\alpha, n\rangle$ through r_{11}, as well as those among $|\beta, n\rangle$ through r_{22}, cancel out to the leading order.

The resonance frequency from Eqs. (A4) and (A5) is

$$\omega_{\mathrm{res}} = E_\beta + \delta_\beta - E_\alpha - \delta_\alpha \simeq E_\beta - E_\alpha + |r_{12}|^2/\omega. \tag{A6}$$

The last term in Eq. (A6) is the rf-induced resonance shift, i.e., the Bloch-Siegert shift (BSS),

$$\delta\omega_{\mathrm{res}} = |r_{12}|^2/\omega. \tag{A7}$$

It is clear that the BSS is induced mostly by the counterrotating component $\bar{B}_1$ of the rf field and disappears if $\bar{B}_1 = 0$ and $\theta = 0$.

Now we consider the energy separation of the two states close to the two-photon resonance, $E_\beta \approx E_\alpha + 2\omega$. In this case, separating the portion of the Floquet Hamiltonian involving the nearly degenerate levels (i.e., finding the corresponding $\mathcal{H}_2$) is less straightforward, as the resonating pairs of states, such as $|\beta, -1\rangle$ and $|\alpha, 1\rangle$, are not directly coupled and are nonresonantly coupled to the nearest intermediate states $|\alpha, 0\rangle$ and $|\beta, 0\rangle$ in addition to the states $|\alpha, -2\rangle$ and $|\beta, 2\rangle$. We find

$$\mathcal{H}_2 = \begin{pmatrix} E_\beta - \omega - \delta_{2p} & u \\ u^* & E_\alpha + \omega + \delta_{2p} \end{pmatrix}, \quad \text{(A8)}$$

where

$$\begin{aligned} \delta_{2p} &= \frac{|r_{12}|^2}{E_\alpha - E_\beta - \omega} + \frac{|r_{21}|^2}{E_\alpha - E_\beta + \omega} \\ &\simeq -\frac{|r_{12}|^2}{3\omega} - \frac{|r_{21}|^2}{\omega}, \\ u &= \frac{r_{21}r_{22}}{E_\alpha - E_\beta + \omega} + \frac{r_{11}r_{21}}{\omega} \\ &\simeq \frac{r_{21}(r_{11} - r_{22})}{\omega}. \end{aligned} \quad \text{(A9)}$$

The resonance frequency of the two-photon transition is thus

$$\begin{aligned} \omega_{\mathrm{res},2p} &= \frac{E_\beta - E_\alpha - 2\delta_{2p}}{2} \\ &\simeq \frac{E_\beta - E_\alpha}{2} + \frac{|r_{12}|^2}{3\omega} + \frac{|r_{21}|^2}{\omega}. \end{aligned} \quad \text{(A10)}$$

In contrast to the BSS of the fundamental resonance, Eq. (A7), the two-photon resonance shift has contributions from both co- and counterrotating components of the rf field,

$$\delta\omega_{\mathrm{res},2p} = \frac{|r_{12}|^2}{3\omega} + \frac{|r_{21}|^2}{\omega}. \quad \text{(A11)}$$

Moreover, as seen from Eq. (A11), in the case of an LP rf field, only 1/4 of the shift comes from the counterrotating component (i.e., r_{12}) whereas 3/4 of the shift comes from the corotating component (r_{21}).

In fact, the first line of Eq. (A9) is universal and describes the leading-order correction to the Floquet energy levels near all higher-harmonic, n-photon resonances for $n \geqslant 2$. In analogy with Eq. (A10), the n-photon resonance occurs when the n-tuple of the frequency is around the energy separation, $n\omega \approx E_\beta - E_\alpha$, or more precisely, at

$$\omega_{\mathrm{res},np} = \frac{E_\beta - E_\alpha - 2\delta_{np}}{n}. \quad \text{(A12)}$$

Utilizing $E_\beta - E_\alpha = n\omega$ in Eq. (A9), the relation for the shift of the n-photon resonance can be expressed as

$$\delta\omega_{\mathrm{res},np} = \frac{2}{n}\left[\frac{|r_{12}|^2}{(n+1)\omega} + \frac{|r_{21}|^2}{(n-1)\omega}\right]. \quad \text{(A13)}$$

The relations derived above can be readily reformulated into forms describing resonance positions as a function of the field B_0 for a fixed rf frequency ω. Neglecting the contribution of the hyperfine field to energy separation and writing $E_\beta - E_\alpha = \gamma B_{\gamma_n}$, we obtain Eqs. (3) and (4).

[1] S. Jamali, V. V. Mkhitaryan, H. Malissa, A. Nahlawi, H. Popli, T. Grünbaum, S. Bange, S. Milster, D. M. Stoltzfus, A. E. Leung *et al.*, Floquet spin states in OLEDs, Nat. Commun. **12**, 465 (2021).

[2] J. P. Ashton and P. M. Lenahan, Multiple-photon transitions in electrically detected magnetic resonance measurements of 4*H*-SiC transistors, Phys. Rev. B **102**, 020101(R) (2020).

[3] F. Bloch and A. Siegert, Magnetic resonance for nonrotating fields, Phys. Rev. **57**, 522 (1940).

[4] V. Hughes and L. Grabner, The radiofrequency spectrum of $Rb^{85}F$ and $Rb^{87}F$ by the electric resonance method, Phys. Rev. **79**, 314 (1950).

[5] L. Grabner and V. Hughes, Further evidence for a two quantum transition in molecular spectroscopy, Phys. Rev. **82**, 561 (1951).

[6] J. Brossel, B. Cagnac, and A. Kastler, Observations de résonances magnétiques à plusieurs quanta sur un jet d'atomes de sodium orientés optiquement, C. R. Acad. Sci. **237**, 984 (1953).

[7] J. H. Shirley, Solution of the Schrödinger equation with a Hamiltonian periodic in time, Phys. Rev. **138**, B979 (1965).

[8] V. N. Ostrovsky and E. Horsdal-Pedersen, Bloch-Siegert shifts and widths for multiphoton resonances: In-plane field configuration, Phys. Rev. A **70**, 033413 (2004).

[9] J. Romhányi, G. Burkard, and A. Pályi, Subharmonic transitions and Bloch-Siegert shift in electrically driven spin resonance, Phys. Rev. B **92**, 054422 (2015).

[10] J. Margerie and J. Brossel, Transitions à plusieurs quanta électromagnétiques, C. R. Acad. Sci. **241**, 373 (1955).

[11] J. Winter, Étude de transitions faisant intervenir plusieurs quanta entre deux niveaux atomiques, C. R. Acad. Sci. **241**, 375 (1955).

[12] C. Cohen-Tannoudji and S. Haroche, Modification et annulation du facteur de Landé d'un atome par couplage avec un champ de radiofréquence, C. R. Acad. Sci., Ser. B **262**, 268 (1966).

[13] C. Cohen-Tannoudji and S. Haroche, Interprétation quantique des diverses résonances observées lors de la diffusion de photons optiques et de radiofréquence par un atome, J. Phys. France **30**, 125 (1969).

[14] V. Morozov, O. Antzutkin, A. Koptyug, and A. Doktorov, Multiquantum resonances in low-field optically detected ESR of radical-ion pairs, Mol. Phys. **73**, 517 (1991).

[15] Y. Sun, Y. Xu, and Z. Wang, The multi-RF photon transition driven by strong RF field in optical magnetic resonance of atoms, Opt. Laser Technol. **145**, 107488 (2022).

[16] D. Fregenal, E. Horsdal-Pedersen, L. B. Madsen, M. Førre, J. P. Hansen, and V. N. Ostrovsky, Multiphoton intrashell resonances in Rydberg atoms: Bloch-Siegert shifts and widths, Phys. Rev. A **69**, 031401(R) (2004).

[17] D. R. McCamey, H. A. Seipel, S.-Y. Paik, M. J. Walter, N. J. Borys, J. M. Lupton, and C. Boehme, Spin Rabi flopping in the photocurrent of a polymer light-emitting diode, Nat. Mater. **7**, 723 (2008).

[18] S. Jamali, G. Joshi, H. Malissa, J. M. Lupton, and C. Boehme, Monolithic OLED-microwire devices for ultrastrong magnetic resonant excitation, Nano Lett. **17**, 4648 (2017).

[19] D. P. Waters, G. Joshi, M. Kavand, M. E. Limes, H. Malissa, P. L. Burn, J. M. Lupton, and C. Boehme, The spin-Dicke effect in OLED magnetoresistance, Nat. Phys. **11**, 910 (2015).

[20] G. Joshi, M. Y. Teferi, R. Miller, S. Jamali, D. Baird, J. van Tol, H. Malissa, J. M. Lupton, and C. Boehme, Isotropic effective

spin-orbit coupling in a conjugated polymer, J. Am. Chem. Soc. **140**, 6758 (2018).

[21] D. M. Stoltzfus, G. Joshi, H. Popli, S. Jamali, M. Kavand, S. Milster, T. Grünbaum, S. Bange, A. Nahlawi, M. Y. Teferi *et al.*, Perdeuteration of poly[2-methoxy-5-(2′-ethylhexyloxy)-1,4-phenylenevinylene] (d-MEH-PPV): Control of microscopic charge-carrier spin–spin coupling and of magnetic-field effects in optoelectronic devices, J. Mater. Chem. C **8**, 2764 (2020).

[22] The NIST reference on constants, units, and uncertainty, deuteron magnetic moment, https://physics.nist.gov/cgi-bin/cuu/Value?mud (Accessed 19 January 2024).

[23] The NIST reference on constants, units, and uncertainty, proton magnetic moment, https://physics.nist.gov/cgi-bin/cuu/Value?mup (Accessed 19 January 2024).

[24] M. Kavand, D. Baird, K. van Schooten, H. Malissa, J. M. Lupton, and C. Boehme, Discrimination between spin-dependent charge transport and spin-dependent recombination in π-conjugated polymers by correlated current and electroluminescence-detected magnetic resonance, Phys. Rev. B **94**, 075209 (2016).

[25] R. Miller, K. J. van Schooten, H. Malissa, G. Joshi, S. Jamali, J. M. Lupton, and C. Boehme, Morphology effects on spin-dependent transport and recombination in polyfluorene thin films, Phys. Rev. B **94**, 214202 (2016).

[26] T. H. Tennahewa, S. Hosseinzadeh, S. I. Atwood, H. Popli, H. Malissa, J. M. Lupton, and C. Boehme, Coherent and incoherent spin-relaxation dynamics of electron-hole pairs in a π-conjugated polymer at low magnetic fields, Phys. Rev. B **109**, 075303 (2024).

[27] E. L. Frankevich, A. A. Lymarev, I. Sokolik, F. E. Karasz, S. Blumstengel, R. H. Baughman, and H. H. Hörhold, Polaron-pair generation in poly(phenylene vinylenes), Phys. Rev. B **46**, 9320 (1992).

[28] C. Boehme and K. Lips, Theory of time-domain measurement of spin-dependent recombination with pulsed electrically detected magnetic resonance, Phys. Rev. B **68**, 245105 (2003).

[29] W. J. Baker, D. R. McCamey, K. J. van Schooten, J. M. Lupton, and C. Boehme, Differentiation between polaron-pair and triplet-exciton polaron spin-dependent mechanisms in organic light-emitting diodes by coherent spin beating, Phys. Rev. B **84**, 165205 (2011).

[30] See Supplemental Material at http://link.aps.org/supplemental/10.1103/PhysRevB.110.195304 for all spectra used for Figs. 3 and 5 and for a version of Fig. 5 with full vertical range.

[31] D. R. McCamey, K. J. van Schooten, W. J. Baker, S.-Y. Lee, S.-Y. Paik, J. M. Lupton, and C. Boehme, Hyperfine-field-mediated spin beating in electrostatically bound charge carrier pairs, Phys. Rev. Lett. **104**, 017601 (2010).

[32] I. Gromov and A. Schweiger, Multiphoton resonances in pulse EPR, J. Magn. Reson. **146**, 110 (2000).

[33] R. C. Roundy and M. E. Raikh, Organic magnetoresistance under resonant AC drive, Phys. Rev. B **88**, 125206 (2013).

[34] F. Wang, C. G. Yang, E. Ehrenfreund, and Z. V. Vardeny, Spin dependent reactions of polaron pairs in PPV-based organic diodes, Synth. Met. **160**, 297 (2010).

[35] T. D. Nguyen, G. Hukic-Markosian, F. Wang, L. Wojcik, X.-G. Li, E. Ehrenfreund, and Z. V. Vardeny, Isotope effect in spin response of π-conjugated polymer films and devices, Nat. Mater. **9**, 345 (2010).

[36] T. D. Nguyen, B. R. Gautam, E. Ehrenfreund, and Z. V. Vardeny, Magnetoconductance response in unipolar and bipolar organic diodes at ultrasmall fields, Phys. Rev. Lett. **105**, 166804 (2010).

[37] S. I. Atwood, V. V. Mkhitaryan, S. Dhileepkumar, C. Nuibe, S. Hosseinzadeh, H. Malissa, J. M. Lupton, and C. Boehme, Three-photon electron spin resonances, Phys. Rev. B **110**, L060103 (2024).

[38] T. Grünbaum, S. Bange, W. Jiang, A. E. Leung, T. A. Darwish, P. L. Burn, and J. M. Lupton, Measuring the magnetic field amplitude of RF radiation by the quasistatic magnetic field effect in organic light-emitting diodes, Phys. Rev. Appl. **15**, 064001 (2021).

[39] W. J. Baker, K. Ambal, D. P. Waters, R. Baarda, H. Morishita, K. van Schooten, D. R. McCamey, J. M. Lupton, and C. Boehme, Robust absolute magnetometry with organic thin-film devices, Nat. Commun. **3**, 898 (2012).

[40] H. Malissa, R. Miller, D. L. Baird, S. Jamali, G. Joshi, M. Bursch, S. Grimme, J. van Tol, J. M. Lupton, and C. Boehme, Revealing weak spin-orbit coupling effects on charge carriers in a π-conjugated polymer, Phys. Rev. B **97**, 161201(R) (2018).